PHYSOR-2006, ANS Topical Meeting on Reactor Physics
Organized and hosted by the Canadian Nuclear Society. Vancouver, BC, Canada. 2006 September 10-14

Short Characteristics Method for Two Dimensional Heterogeneous Cartesian Cells

Emiliano Masiello, Igor Zmijarevic
CEA de Saclay, 91190 Gif sur Yvette, CEDEX France
e-mail: emiliano.masiello@cea.fr, igor.zmijarevic@cea.fr

Abstract

The short characteristics method for two-dimensional xy-geometry is extended to heterogeneous Cartesian cells. The new method is intended for realistic neutron transport calculation, as for pressurized water reactor assemblies and bundles, without pin cells homogenization. The pin cell is chosen as the basic element for geometrical mapping. Thus, the heterogeneous cells are modeled by a rectangular element with an arbitrary number of concentric rings. Test problems show that the use of this kind of cells allows a minimal geometrical modeling without a significant lost in precision.

KEYWORDS: Short characteristics method, Discrete ordinate method, Boundary projection acceleration, Coarse mesh finite difference, Interface flux discontinuity factor

1. Introduction

The method of short characteristics has been proposed in the early 80's for the solution of the xy-geometry discrete ordinate neutron transport equation. [1] The method is based on the use of the integral form of the transport equation as exact propagation equation throughout Cartesian cells, while the angular flux and the sources are expanded in each cell on polynomial base functions. Compared to the finite differences and nodal method approximations this gives a more precise spatial dependency of sources and a better description of the attenuation across the mesh cells.

In this paper, we present a short characteristics method applied to Heterogeneous Cartesian Cells (HCC). The method has been incorporated into the discrete ordinates IDT solver of the APOLLO2 lattice code. [2] [3] [4] The IDT solver treats 2D and 3D Cartesian geometries with arbitrary anisotropy of scattering and provides spatial solutions by two methods, i.e., the nodal and the short characteristics method, with a maximum spatial expansion up to the bilinear order for the volume flux and a linear expansion for the surface flux in 2D.

The introduction of 2D HCC, as a basic tool for geometrical modeling, enables the application of the IDT code to the study of PWR assemblies and bundles in the exact geometry. The HCC is composed by an external rectangular surface containing an arbitrary number of concentric, homogeneous rings. The flux is expanded in polynomial base functions locally defined on each region composing the cell and on the sides of the rectangle. The discretized transport equation is given by two linear systems similar to those for the homogeneous cells of IDT. For a given direction, these systems link the volume spatial moments and the outgoing surface spatial moments to the source moments and incoming flux surface moments. The basic S_N

solution algorithm is unchanged, the transmission of the outgoing flux is performed in the same way as for the homogeneous cells. Thus, the numerical scheme preserves the typical fast resolution of the discrete ordinates method on Cartesian meshes.

Figure 1: Heterogeneous Cartesian Cell and its integration scheme. The discontinuities of the cell are projected and the quadrature points are distributed on the perpendicular plane represented by the segment $\overline{AB}$.

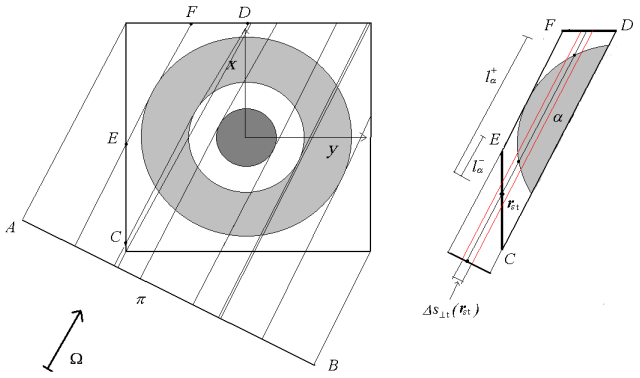

2. Heterogeneous cells

We consider the one-group transport equation for a fixed direction Ω belonging to the set of directions defined by the S_N angular quadrature formula. The in-group source $q(\mathbf{r}, \Omega)$ comprises the self-scattering contribution and the external sources. The scattering source is angularly expanded on the spherical harmonic base functions. The S_N Source Iterations (SI) algorithm proceeds by sweeping the domain in each direction and updating the angular flux moments needed for the construction of the new source.

We seek an approximated solution of the one-group transport equation on a HCC with an arbitrary number M of homogeneous regions (see Fig. 1). We proceed with a Galerkin projection of the integral form of the transport equation on each volume D_α and on each outgoing surface $\Gamma_{s'}^+$,

$$\begin{aligned} \psi(\mathbf{r}) &= \psi(\mathbf{r}_s)e^{-\tau(l,0)} + \int_0^l dl' q(\mathbf{r}')e^{-\tau(l,l')}, \quad \mathbf{r} \in D_\alpha \\ \psi(\mathbf{r}_{s'}) &= \psi(\mathbf{r}_s)e^{-\tau(L,0)} + \int_0^L dl' q(\mathbf{r}')e^{-\tau(l,l')}, \quad \mathbf{r}_{s'} \in \Gamma_{s'}^+ \end{aligned} \tag{1}$$

here α is the index of the internal regions, while s and s' are, respectively, the index of the entering and exiting sides of the rectangle. The integral transport equation is written on a trajectory intersecting the cell, $\mathbf{r}_s$ is an entering surface point, while $\mathbf{r}=\mathbf{r}_s + \Omega l$, $\mathbf{r}'=\mathbf{r}_s + \Omega l'$, and $\mathbf{r}_{s'}=\mathbf{r}_s + \Omega L$ are respectively a volume interior point, a generic point , and an exiting surface point laying on the trajectory. For the sake of simplicity, we intentionally omit the angular dependency which we supposed be fixed by the quadrature formula. The flux and the source are expanded in each region D_α

$$\psi(\mathbf{r}) = \psi_\alpha \cdot \mathbf{p}_\alpha(\mathbf{r}) \quad , \quad q(\mathbf{r}) = \mathbf{q}_\alpha \cdot \mathbf{p}_\alpha(\mathbf{r}), \tag{2}$$

where $\mathbf{p}_\alpha(\mathbf{r})$ is the finite orthonormal polynomial basis defined on D_α. In our case $\mathbf{p}_\alpha(\mathbf{r})$ contains at most the bilinear polynomial. The vectors ψ_α, $\mathbf{q}_\alpha$ contain respectively the spatial moments of the flux and the spatial moments of the source relative to a region α:

$$\psi_\alpha = (\mathbf{p}_\alpha, \psi)_\alpha = \int_{D_\alpha} d\mathbf{r}\ (\mathbf{p}_\alpha \psi)(\mathbf{r}) \quad \text{and} \quad \mathbf{q}_\alpha = (\mathbf{p}_\alpha, q)_\alpha = \int_{D_\alpha} d\mathbf{r}\ (\mathbf{p}_\alpha q)(\mathbf{r}). \tag{3}$$

In a similar manner the surface flux is expanded on the exiting and the entering sides

$$\psi^+(\mathbf{r}_{s'}) = \psi^+_{s'} \cdot \mathbf{p}_{s'}(\mathbf{r}_{s'}), \quad \psi^-(\mathbf{r}_s) = \psi^-_s \cdot \mathbf{p}_s(\mathbf{r}_s). \tag{4}$$

The incoming flux moments $\psi^+_{s'}$ and the exiting flux moments ψ^-_s are computed by the surface scalar products

$$\begin{aligned} \psi^+_{s'} &= < \mathbf{p}_{s'}, \psi >^+_{s'} = \int_{\Gamma_{s'}} d\Gamma\ |\Omega \cdot \mathbf{n}_{s'}|\, (\mathbf{p}_{s'} \psi)(\mathbf{r}) \\ \text{and}\quad \psi^-_s &= < \mathbf{p}_s, \psi >^+_s = \int_{\Gamma_s} d\Gamma\ |\Omega \cdot \mathbf{n}_s|\, (\mathbf{p}_s \psi)(\mathbf{r}). \end{aligned} \tag{5}$$

The projection of the integral equations (1) on the volume and on the surface base functions, respectively, leads to an explicit linear system which relates the interior and the exiting flux to the incoming flux and sources

$$\begin{aligned} \psi &= C\mathbf{q} + I\psi^-, \\ \psi^+ &= E\mathbf{q} + T\psi^-. \end{aligned} \tag{6}$$

Here, the vector $\psi = \{\psi_\alpha,\ \alpha = 1, M\}$ contains the volume spatial moments of the flux, $\mathbf{q} = \{\mathbf{q}_\alpha,\ \alpha = 1, M\}$ represents the volume spatial moments of the sources and $\psi^\pm = \{\psi^\pm_{s'/s},\ s', s = 1, 4\}$ are the surface spatial moments on the entering and exiting sides of the cell. The matrices appearing in Eqs. (6) have an explicit meaning:

– $C(\Omega)$ is the collision matrix, i.e., $C(\Omega) = \{C_{\alpha\beta}(\Omega),\ \alpha, \beta = 1, M\}$, where each submatrix

$$C_{\alpha\beta}(\Omega) = (\mathbf{p}_\alpha, e^{-\tau_{\alpha\beta}} \mathbf{F}_\beta)_\alpha \tag{7}$$

relates the source moments in region β to the flux in region α. The exponential function vector $\mathbf{F}_\alpha(l)$ is given by the integral $\mathbf{F}_\alpha(l) = \int_{l^-_\alpha}^{l} dl' e^{-\Sigma_\alpha(l-l')} \mathbf{p}_\alpha$.

– $I(\Omega)$ is the incoming matrix, i.e., $I(\Omega) = \{I_{\alpha s}(\Omega),\ s = 1, S^-\ \alpha = 1, M\}$, where

$$I_{\alpha s}(\Omega) = (\mathbf{p}_\alpha, e^{-\tau_{\alpha s}} \mathbf{p}_s)_\alpha \tag{8}$$

takes into account the contribution from the entering side s to region α.

– $E(\Omega)$ is the outgoing matrix, $E(\Omega) = \{E_{s'\alpha}(\Omega)\ s' = 1, S^+\ \alpha = 1, M\}$, each submatrix

$$E_{s'\alpha}(\Omega) = < \mathbf{p}_{s'}, e^{-\tau_{s'\alpha}} \mathbf{F}_\alpha >^+_{s'} \tag{9}$$

relates region α to the outgoing surface s'.

– Finally the transmission matrix $T(\Omega) = \{T_{s's}(\Omega),\ s' = 1, S^+,\ s = 1, S^-\}$, where

$$T_{s's}(\Omega) = < \mathbf{p}_{s'}, e^{-\tau_{s's}} \mathbf{p}_s >^+_{s'} \tag{10}$$

takes into account the transmission of particles between sides s and s'.

These matrices respect conservation and reciprocity relations which can be used to renormalize the coefficients. We have explicitly shown the angular dependence of the matrices due to the attenuation coefficients $e^{-\tau}$ which unables matrix factorization. The four matrices are stored for each HCC as well as for each energy group and angular direction. Equations (6) are used for the transport sweep in a Cartesian mesh.

2.1 Spatial integration

Because of the interior rings, the matrix coefficients cannot be analytically integrated. The integrals appearing in the definition of the spatial coefficients, Eq.s (7)-(10), can be split into an analytical part along the trajectory and a numerical part along the perpendicular plane (see Fig. 1). The volume and surface scalar products (3) and (5) are computed by a quadrature formula:

$$(\mathbf{p}_\alpha, \psi)_\alpha = \sum_{t \cap \alpha} \Delta s_{\perp t} \int_{l_\alpha^-}^{l_\alpha^+} dl \; (\mathbf{p}_\alpha \psi)(\mathbf{r}_{st} + l\Omega), \tag{11}$$

$$\begin{aligned} < \; \mathbf{p}_{s'}, \psi >_{s'}^{+} &= \sum_{t \cap s'} \Delta s_{\perp t} \; (\mathbf{p}_{s'} \psi)(\mathbf{r}_{st} + L\Omega), \\ < \; \mathbf{p}_{s}, \psi >_{s}^{-} &= \sum_{t \cap s} \Delta s_{\perp t} \; (\mathbf{p}_{s} \psi)(\mathbf{r}_{st}), \end{aligned} \tag{12}$$

where t is the index of the set of trajectories parallel to Ω used for the integration, $\Delta s_{\perp t}$ is the perpendicular weight area associated to the trajectory and $\mathbf{r}_{st}$ is the surface quadrature point. The tracking technique is similar to that used in the collision probability and in the step characteristics methods. In particular, the perpendicular surface is divided into intervals that respect the geometrical discontinuities and a Gauss-Legendre quadrature is used on each interval. The coefficients of matrices C, I, E and T are obtained by a linear combination of recursive exponential integral functions along the trajectory and a numerical integration along the perpendicular surface (the segment $\overline{AB}$ in Fig. 1).

A Gram-Schmidt procedure is used to numerically orthonormalize the base expansion functions according to scalar products (11) and (12). Thus, the computed base coefficients depend on the numerical quadrature formula and, implicitly, on the direction. The angular dependency of the base coefficients have to be as weak as possible in order to define a unique spatial representation for all angular directions. In our experience, numerical tests have shown that 10 surface intervals with a minimum tracking spacing of 0.05 cm are sufficient to guarantee the construction of a direction-independent expansion base with a precision of 10^{-8} on the coefficients.

Another important remark is relative to numerical conservation. The projection of the integral equation using numerical integration can lead to errors in the balance equation. In our case, we use numerical spatial integrations as projector operator as well as numerical scalar product for the Gram-Schmidt orthogonalization procedure. Because the latter is consistent with the projector operator, the resulting matrices C, I, E and T preserve automatically the balance equation. In our experience, and although we do not have a rigorous mathematical demonstration, we have observed that conservation is respected even when using only one point quadrature formula, so the matrices need no renormalization. However, we cannot use coarse quadrature formulas because of the risk of direction-dependent spatial base functions, which would lead to errors in the computation of the scattering source.

Finally, the matrices are computed for all directions in the azimuthal angular interval $[0, \pi]$, while for the remaining interval $[\pi, 2\pi]$ they are obtained by the formulas

$$\begin{aligned} C_{\alpha\beta}(-\Omega) &= C^T_{\beta\alpha}(\Omega), \;\; I_{\alpha s'}(-\Omega) = E^T_{s'\alpha}(\Omega) \\ E_{s\alpha}(-\Omega) &= I^T_{\alpha s}(\Omega), \;\; T_{ss'}(-\Omega) = T^T_{s's}(\Omega), \end{aligned}$$

derived from reciprocity relations.

3. Discontinuous surface expansion

Suppose we analyze a transmission problem in a pure absorber, as depicted in Fig. 2, with an incoming surface source positioned on the left bottom side of the geometry at 45° on the azimuthal plane. Then, the analytical exiting flux on the top surface is given by the exponential shape shown in Fig. 2. The numerical solution given by the short characteristics on a 3×3 coarse mesh is affected by numerical diffusion due to the transmission of unphysical surface flux moments (see Fig. 2 C1) and the resulting exiting flux has a shape distributed along all the surface of the side (top side of the geometry).

Obviously, numerical diffusion can be attenuated using finest meshes. In our case, instead of refining everywhere the meshes, one introduces a local uniform partition on the internal and external surfaces of the mesh. More precisely, each side L_s is subdivided in K equal intervals in which the flux is locally expanded. Thus, instead of Eq. (4), we define a discontinuous surface expansion

$$\psi^{+}(\mathbf{r}_{s'}) = \sum_{k=1}^{K} \psi^{+}_{s'k} \cdot \mathbf{p}_{s'k}(\mathbf{r}_{s'}), \quad \psi^{-}(\mathbf{r}_{s}) = \sum_{k=1}^{K} \psi^{-}_{sk} \cdot \mathbf{p}_{sk}(\mathbf{r}_{s}),$$

where $\mathbf{p}_{s/s'k}$ are the Legendre polynomial bases defined on the surface interval k of the side s/s', while $\psi^{\pm}_{sk}$ are the related surface spatial moments. The discontinuous surface expansion can reduce numerical diffusion effects (see Fig. 2 C2-6) so that the error is propagated only throughout the shadowed intervals of the exiting sides, limiting, thus, numerical pollution.

This refined boundary expansion does not result in a dramatic increase of storage. Although the transmission matrix increases its dimensions by a factor K^2, and the escape and the incoming matrices by a factor K, the number of zero elements also increases with the number of surface intervals, so the storage can be consistently reduced. In the implementation of the method in the IDT solver the user can arbitrary choose the number of surface intervals and the order of surface and volume expansion depending on the nature of the problem.

4. Acceleration methods

4.1 The Boundary Projection Acceleration preconditioned by Non Linear Diffusion

Two types acceleration techniques for the inner iterations have been originally implemented in the IDT solver, namely, the Boundary Projection Acceleration (BPA) and the Diffusion Synthetic Acceleration (DSA), both for homogeneous cells. [2] [3] [5] A spatial Multi Grid algorithm (MG) on the diffusion operator is also available to accelerate the DSA solution.

We have extended the BPA matrices to the HCC formalism. The BPA sweep is still done on a S_2 angular grid using an ADI algorithm, which is very costly for HCCs with several regions. In order to attenuate high and low frequencies of the error spectrum we have preconditioned the BPA with a non-linear diffusion operator. The diffusion operator is constructed by introducing flux-weighted homogeneous cross sections in each cell with the dynamical homogenization of the HCCs. The residual of the angular moments $\Delta\phi_i^{\alpha} = \phi_i^{\alpha(l+1)} - \phi_i^{\alpha(l)}$, where l is the inner iteration index, is homogenized by a volume-weighted technique and transferred to the diffusion operator as the source. After a transport iteration, one constructs the residual and performs a partially converged BPA sweep and the resulting system is solved by ADI. Finally, the corrected moments vector $\phi_{ACC}^{\alpha,(l+1)}$ is computed by adding the error $\phi_{\varepsilon}^{\alpha,BPA}$, given by the

Figure 2: Simple transmission test problem in a pure absorber. A) test problem, B) Analytical shape of the angular flux at the top side of the geometry for an angle of 45° on the azimuthal plane at 36° with respect to the polar axis (central angle of the S4 level symmetric quadrature formula). C1-6) Numerical solutions with constant expansion obtained respectively with 1, 2, 3, 4, 6, and 8 surfaces per cell side.

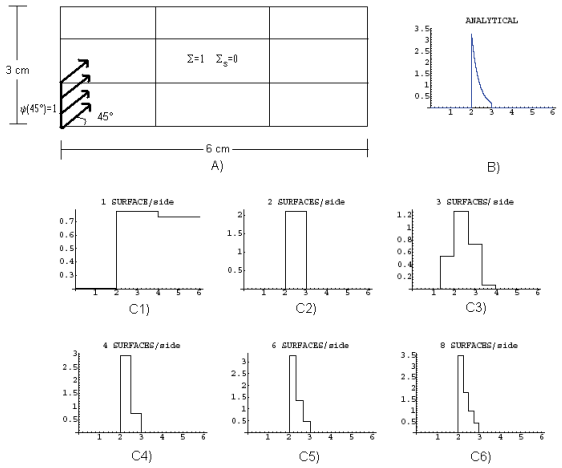

BPA, and the error $\phi^{NLD}_{\varepsilon,\mathrm{hom}}$ of the non-linear diffusion operator to flux moments $\phi^{\alpha,(l+1)}$

$$\phi^{\alpha,(l+1)}_{ACC} = \phi^{\alpha,(l+1)} + \phi^{\alpha,BPA}_{\varepsilon} + f^{\alpha}\phi^{NLD}_{\varepsilon,\mathrm{hom}}.$$

Here f^{α} is the shape factor defined by the ratio

$$f^{\alpha} = \frac{\phi^{\alpha}}{\phi_{\mathrm{hom}}}, \tag{13}$$

where ϕ_{hom} is the homogenized flux relative to the HCC.

4.2 The CMFD and the IFDF non linear techniques

We speed up the source iteration acceleration algorithm by introducing two types of non-linear operators: the Coarse Mesh Finite Difference technique (CMFD) and Interface Flux Discontinuity Factors (IFDF). [7] [8]

Both methods are characterized by the first-moment finite-difference balance equation:

$$(J^R - J^L)L_y + (J^T - J^B)L_x + V\Sigma\phi_{\mathrm{hom}} = Vq_{\mathrm{hom}}, \tag{14}$$

where:

– J^R, J^L, J^T and J^B are the net currents relative to the right, left, top, and bottom side of the Cartesian cell

– L_y, L_x are the x and y side,

– V is the total volume of the cell, $V = \sum_{\alpha} V_{\alpha}$,

– Σ is the flux-weighted homogenized cross section.

Finite difference equation (14) is obtained by collapsing the HCC balance equation to the zero-order spatial moment over the cell. With these spatially homogenized constants, the problem would not converge on the same node average flux distribution given by the transport

operator. The equivalent finite difference problem can be established only when the interface currents of the transport reference solution, i.e., $J^{R/L/T/B}$, are preserved. To this end, two different relations are used respectively for the CMFD and the IFDF. For the CMFD, the net current is computed using the finite differenced current relation. For example, the current-flux relation on the right side of the cell reads

$$J^R = -\frac{D}{L_x}(\phi^R_{\rm hom} - \phi_{\rm hom}) + \frac{\widetilde{D}^R}{L_x}(\phi^R_{\rm hom} + \phi_{\rm hom}), \tag{15}$$

where $\phi^R_{\rm hom}$ is the average flux of the right neighbour cell. Among the two diffusion coefficients appearing in Eq. (15), the first one is determined by flux-weighting the diffusion coefficients of the regions composing the HCC and, in order to force the interface current to be the same as the transport current, the second one is computed from the transport solution:

$$\widetilde{D}^R = \frac{J^R + D(\phi^R_{\rm hom} - \phi_{\rm hom})}{\phi^R_{\rm hom} + \phi_{\rm hom}},$$

where all quantities J^R, $\phi^R_{\rm hom}$ and $\phi_{\rm hom}$ are computed after a transport sweep. Thus, each side of the cell defines a different coefficient $\widetilde{D}$.

Instead of adding a diffusion coefficient in the diffusion Fick's law, for the IFDF one corrects locally the finite difference approximation of the flux gradient at the mesh interface, so that the net current is related to the difference of the actual cell average and modified cell interface fluxes, i.e.,

$$J^R = -\frac{D}{L_x/2}(f^R\phi^R - \phi_{\rm hom}). \tag{16}$$

Here ϕ^R is the interface scalar flux relative to the right side, while f^R is the discontinuity factor that forces the finite difference interface current to be the same as the transport current. More precisely, this factor is computed as

$$f^R = \frac{\phi_{\rm hom} - L_x J^R/2D}{\phi^R}.$$

A few remarks have to be done. At each transport sweep, one stores the net current and the boundary flux for each side of the cells. Only the constant spatial moment is corrected properly for both methods. The linear and bilinear spatial moments are corrected by reconstructing the flux gradients in the x and y directions using the actual average homogenized flux $\phi_{\rm hom}$ and the four surface fluxes $\phi^{R/L/T/B}$. Moreover, both methods lead to a five-diagonal matrix that, in our case, is inverted with the BiCGSTAB algorithm without preconditioning or by a Multigrid in which each grid matrix is solved with ADI. As long as the diagonal dominance is not lost, the fast convergence to the iterative solution of the linear system is preserved. This particular propriety of the matrix is especially necessary to stabilize the ADI solver. This implies that the corrected diffusion coefficients $\widetilde{D}$, as well as the discontinuity factors f, are positive and bounded. Such conditions can be guaranteed by imposing bounding values to the homogenized diffusion coefficient. [8] The shape factor introduced in Eq. (13) are also used to correct the heterogeneous flux .

We have also extended the CMFD scheme to the multigroup iterations, which involves a dynamical homogenization of the multigroup cross sections. During an outer iteration, a transport

Table 1: 17x17 MOX assembly calculation with 2-ring HCCs with linear expansion. BPA = SI accelerated by Boundary Projection, BPA-NLD = SI accelerated by BPA and preconditioning by Non Linear Diffusion, IFDF = SI accelerated by IFDF. CMFD = SI accelerated by CMFD and solved by BiCGSTAB, CMFD-MG = inners iterations accelerated by CMFD and solved by Spatial Multi Grid. CMFD-external = both multigroup and source iterations accelerated by CMFD and solved by BiCGSTAB.

	# inners	# outers	CPU (s)	k-eff
free it.	1004	9	25.4	1.18240
BPA	344	21	15.6	1.18239
BPA-NLD	230	19	9.7	1.18239
IFDF	182	13	4.6	1.18245
CMFD	133	19	6.3	1.18235
CMFD-MG	91	13	3.2	1.18236
CMFD-external	74	6	3.4	1.18242

multigroup sweep and a non linear diffusion solution are succesively done. At each transport multigroup sweep, the multigroup interface fluxes and currents are stored to build the homogenized multigroup constants that enforce balance (see [9] for more details).

5. Numerical Results

5.1 A 7-group PWR MOX assembly

Table I summarizes the performance of the above mentioned acceleration techniques for a 7 group PWR 17x17 MOX assembly calculation. [10] The assembly is studied in its whole geometry, without taking advantage of the geometrical symmetry, and it is discretized by 17x17 HCCs involving 3 regions per pin (2 rings). The angular quadrature is a S_{16} level symmetric quadrature formula. All the calculations were run on a laptop Intel Pentium(R) 1.4-GHz 512-Mo. The CMFD algorithm has been proved to be the most efficient of the three analyzed algorithms, mainly because the resulting diffusion matrix is more easily inverted. We note also that the multigroup CMFD reduces by a factor of 3 the number of external iterations with respect to the CMFD solved with BiCGSTAB alone. However, the resulting multigroup diffusion operator can lead to an ill conditioned matrix, especially at the first external iterations, when the transport operator is far from convergence. We think that a good initialization of the multigroup transport iterations followed by a proper preconditioning of the matrix can improve the efficiency of the method in terms of CPU time.

5.2 The C5G7MOX benchmark

We analyze the well known NEA/OECD C5G7MOX 2D benchmark, [10], using two types of heterogeneous cells with one and two rings, respectively, to model the fuel-pin. Comparisons are done with the reference Monte Carlo calculation, and a S_8 short characteristics calculation using a 722500-region mesh of homogeneous Cartesian cells with an approximated representation of the pin cells.

The two meshes are composed by four assemblies discretized with 17x17 HCCs with a total of 3757 regions using one ring and a total of 4913 regions using 2 rings, while the reflector is described with homogeneous cells. Calculations are done for the constant, the linear and

Table 2: C5G7MOX benchmark results. MC = MonteCarlo. IDT = short characteristic with homogeneous cell and a linear expansion. IDT-n rings= short characteristic with HCCs. n = spatial order 0 = constant, 1 = linear, 2 = bilinear. The error is computed with respect to the MC calculation.

Calculation	# reg.	n.	# it.	CPU(s)	RMS(%)	K- inf	err.(%)	$\Delta\rho$(pcm)
MC	—	–	—	—	—	1.18655	—	—
IDT	722500	1	1634	14379	—	1.18520	—	-113
IDT-1 ring	3757	0	1369	114	3.21	1.18225	-7.54	-362
		1	233	59	0.59	1.18647	-1.62	-7
		2	233	68	0.41	1.18644	-1.12	-9
IDT-2 rings	4913	0	1407	136	2.67	1.18231	-6.32	-357
		1	240	77	0.45	1.18650	0.81	-4
		2	237	94	0.32	1.18649	0.48	-5

the bilinear flux expansions, while a unique S_8 level symmetric quadrature formula is used to discretize the angular variable. The source iterations are accelerated by CMFD solved with a spatial multigrid. The matrix coefficients are computed and stored for each pin type, in particular 7 matrices are computed and stored for each group, 1 for the homogeneous cell and 6 for heterogeneous cells. All the calculations were run on a laptop Intel Pentium(R) 1.4-GHz 512-Mo. In Table 2 are summarized the results of the above mentioned calculations, while Fig. 3 depicts the percent error over the 2x2 central bundle using 2 rings HCCs with bilinear expansion .

The HCCs enable a good representation of the flux in the pin cells, especially using linear or bilinear expansions. The latter produce a maximal error on the fission rate lesser than 2% using 1 ring, and lesser than 1% using 2 rings, demonstrating the good accuracy of the method.

Figure 3: Percent relative error between Monte Carlo calculation and a S8-IDT calculation using bilinear expansion and HCCs with 2 rings.

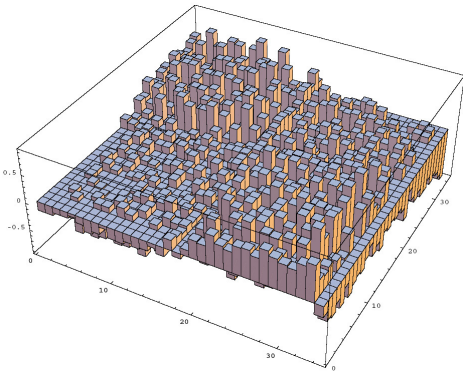

6. Conclusion

We have implemented a novel Heterogeneous Cartesian Cell in the xy-geometry solver of the APOLLO2 code. We have written the final discretized equations in the same form as

for the homogeneous Cartesian cells, preserving, thus, the fast solution given by the standard S_N transport sweep. The HCC is also an interesting tool to reduce the need of geometrical modeling without recurring to spatial homogenization. Moreover, numerical tests show that there is no appreciable loss in precision, especially using linear or bilinear expansions.

Memory requirements due to storage of coefficients can be significantly large. The storage is minimized by considering only cells with different optical dimensions and either store or compute on the fly the corresponding matrix coefficients for any set of energy groups.

The HCCs could also be generalized to non-conforming Cartesian meshes, allowing, thus, the analysis of more complex assembly geometries, as those of BWR assemblies.

Others important improvements can be realized to accelerate the iterative scheme, in particular for the inversion of the finite difference matrix. In future work, we will try to apply the MG solver with a preconditioner for a faster inversion of the multigrup CMFD operator.

Acknowledgements

The authors wish to thank Richard for providing the tracker.

References

1) Larsen, E.W., Alcouffe, R.E., ”The linear characteristic method for spatially discretizing the discrete ordinates equations in (x,y)-geometry.” Proc. Int. Topl. Mtg. on Advances in Math. Methods for the Solution of Nucl. Eng. Problems, Munich, Germany, April 27-29, 1981, American Nuclear Society.

2) Zmijarevic, I., ”Multidimensional discrete ordinates nodal and characteristics methods for APOLLO2 Code”, Proc. Mathematics & Computation, Reactor Physics and Enviromental Analysis in Nuclear Applications, Madrid, Spain, September 1999, 705 (1999).

3) Zmijarevic, I., Sanchez, R., Lamponi, D., ”Diffusion synthetic acceleration of linear nodal schemes in weighted difference form”, Proc. ANS Int. Mtg. on Mthematical Methods for Nuclear Applications, Salt Lake City, USA, September 2001.

4) Sanchez, R., et al., ”APOLLO II: A user–oriented, portable, modular code for multigroup transport assembly calculations”, Nuc. Sci. Eng. **100**, 352 (1988).

5) Adams, M.L., Martin, W.R., ”Boundary projection acceleration: a new approach to synthetic acceleration of transport calculations”, Nuc. Sci. Eng. **100**, 177 (1988).

6) Smith, K. S., Henry, A. F., Loretz, R., ”Determination of homogenized diffusion theory parameter for coarse mesh nodal analysis”, Proc. ANS Topl. Mtg. Advanced in Reactor Phsics and Shielding, Sun Valley, Idaho, September 14-19, 1980, 224, ANS (1980).

7) Aragonés, J. M., Ahnert, C., ”A linear discontinous finite difference formulation for synthetic coarse-mesh few-group diffusion calculations”, Nuc. Sci. Eng. **94**, 309 (1986).

8) Joo, H. J., et al., ”Dynamic implementation of the equivalence theory in the heterogeneous whole core transport calculation”, PHYSOR 2002, Seoul, Korea, October 7-10,2002, 447 (2002).

9) ”AEN/ NEA Benchmark on deterministic transport calculation without spatial homogenization”, Nuclear Science, OECD, Paris (2003).